Received: 7 August 2020 | Accepted: 19 October 2020

DOI: 10.1111/ene.14609

european journal of neurology
the official journal of the european academy of neurology

ORIGINAL ARTICLE

Associations between texture of T1-weighted magnetic resonance imaging and radiographic pathologies in Alzheimer's disease

Subin Lee[1] | Ki Woong Kim[1,2,3] | for the Alzheimer's Disease Neuroimaging Initiative*

[1]Department of Brain and Cognitive Sciences, Seoul National University College of Natural Sciences, Seoul, Korea

[2]Department of Neuropsychiatry, Seoul National University Bundang Hospital, Seongnam, Korea

[3]Department of Psychiatry, Seoul National University College of Medicine, Seoul, Korea

Correspondence
Ki Woong Kim, Department of Neuropsychiatry, Seoul National University Bundang Hospital, 82 Gumi-ro 173 beon-gil, Bundang-gu, Seongnam-si, Gyeonggi-do 13620, Korea.
Email: kwkimmd@snu.ac.kr

Funding information
Institute for information and communications technology, Republic of Korea, Grant/Award Number: 2018-2-00861; Ministry of Health and Welfare, Republic of Korea, Grant/Award Number: HI09C1379 [A092077]; Alzheimer's Disease Neuroimaging Initiative (ADNI); National Institutes of Health Grant, Grant/Award Number: U01 AG024904; Department of Defense, Grant/Award Number: W81XWH-12-2-0012; National Institute on Aging; National Institute of Biomedical Imaging and Bioengineering

Abstract

Background and purpose: Texture analysis of magnetic resonance imaging (MRI) brain scans have been proposed as a promising tool in the early diagnosis of Alzheimer's disease (AD), but its biological correlates remain unknown. In this study, we examined the relationship between MRI texture features and AD pathology.

Methods: The study included 150 participants who had a 3.0T T1-weighted image, amyloid-β positron emission tomography (PET), and tau PET within 3 months of each other. In each of six brain regions (hippocampus, precuneus, and entorhinal, middle temporal, posterior cingulate and superior frontal cortices), linear regression analyses adjusting for age and sex was performed to examine the effects of regional amyloid-β and tau burden on regional texture features. We also compared neuroimaging measures based on pathological severity using ANOVA.

Results: In all regions, tau burden ($p < 0.05$), but not amyloid-β burden, were associated with a certain texture feature that varied with the region's cytoarchitecture. Specifically, autocorrelation and cluster shade were associated with tau burden in allocortical and periallocortical regions, whereas entropy and contrast were associated with tau burden in neocortical regions. Mean signal intensity of each region did not show any associations with AD pathology. The values of the region-specific textures also varied across groups of varying pathological severity.

Conclusions: Our results suggest that textures of T1-weighted MRI reflect changes in the brain that are associated with regional tau burden and the local cytoarchitecture. This study provides insight into how MRI texture can be used for detection of microstructural changes in AD.

KEYWORDS
Alzheimer's disease, cytoarchitecture, magnetic resonance imaging, tau, texture

INTRODUCTION

Alzheimer's disease (AD) is characterized by progressive accumulation of amyloid-β (Aβ) and tau, followed by atrophy. Although structural magnetic resonance imaging (MRI) is a noninvasive, less costly, and widely available tool for observing neurodegenerative changes in AD, its use has been mainly limited to detecting macroscopic structural changes (local brain volume), which occur long after microscopic changes associated with protein deposits have occurred in the AD brain.

Recently, a series of studies have shown promising results that texture analysis of MRI can detect AD earlier than when using volume-based measures. Texture analysis describes spatial patterns of signal intensity variations within an image in quantitative metrics. Early studies reported significant group differences in various

*Data used in preparation of this article were obtained from the Alzheimer's Disease Neuroimaging Initiative (ADNI) database (adni.loni.usc.edu). As such, the investigators within the ADNI contributed to the design and implementation of ADNI and/or provided data but did not participate in analysis or writing of this report. A complete listing of ADNI investigators can be found at: http://adni.loni.usc.edu/wp-content/uploads/how_to_apply/ADNI_Acknowledgement_List.pdf

texture features among cognitively normal (CN) participants, patients with mild cognitive impairment (MCI), and AD [1, 2]. Later studies reported that individual texture features and optimally combined indices could discriminate patients with AD from CN with good accuracy [3–9], and recent studies showed that texture could predict AD progression from patients with MCI better than hippocampal volume can [6, 7, 9], suggesting the potential of texture to reflect microstructural changes beyond macroscopic ones such as atrophy. The AD predictive performance of texture in these studies [6, 7] is one of the highest reported among structural MRI markers.

However, despite the demonstrated capabilities of texture in the diagnosis and prognosis of AD, there is yet a lack of fundamental understanding of the neuropathological and biological correlations between MRI texture and AD-affected brain tissue. Several factors are known to influence and determine signal intensity in T1-weighted images, such as the local biochemical environment, cytoarchitecture, and myeloarchitecture [10, 11]. As such, accumulations of AD pathology (Aβ and tau burden) can cause changes in tissue microstructure overtime, which can lead to an alteration of its signal intensity distribution (texture). Furthermore, the pattern and degree of texture changes may be different with respect to the region's underlying cytoarchitecture. Currently, there have been no direct investigations of this in the human brain.

This study aimed to examine the associations of regional texture features of T1-weighted MRI with regional Aβ and tau burdens, as measured by positron emission tomography (PET). We investigated these associations in each of cytoarchitecturally different brain regions that are involved in early to late phases of AD pathology (hippocampus, precuneus, and entorhinal, middle temporal, posterior cingulate, and superior frontal cortices) [12, 13]. We also compared neuroimaging measures between groups based on level of pathological burden. We hypothesized that Aβ and/or tau accumulation may change MRI texture, and that the affected texture feature will be different between pathological stages and between cytoarchitecturally different brain regions.

METHODS

Study participants

We retrospectively interpreted prospectively acquired data from January 2017 to October 2018 from the Alzheimer's Disease Neuroimaging Initiative 3 (ADNI 3) database, downloaded on 11 November 2018. ADNI 3 was approved by the institutional review board at each site, and all participants gave their written consent. For information on diagnostic criteria, see www.adni-info.org. We included participants who had a 3.0T T1-weighted MRI obtained from a Siemens scanner, an F^{18}-AV45 (florbetapir) PET scan, and an F^{18}-AV1451 (flortaucipir) PET scan, all taken within 3 months of each other regardless of their clinical diagnoses. Because texture features are known to be affected by MRI scanner platforms [14], we focused our study on T1-weighted images obtained from only one type of scanner (Siemens) that created the majority of the ADNI 3 images (Siemens, $n = 150$; GE, $n = 66$; Philips, $n = 17$), resulting in 150 participants total. Intervals between different image modalities ranged from 12.5 to 22.5 days average.

For group comparison, we divided the participants based on Braak stages, which is a method of staging the severity of AD based on topographic patterns of AD pathological burden in the brain. In our study, we determined each participant's Braak stage in vivo using a PET-based method [15], which is described in Data S1 and S2.

Regions of interest

The regions of interest (ROIs) included the hippocampus (HPC), entorhinal cortex (ERC), middle temporal cortex (MTC), posterior cingulate cortex (PCC), precuneus (PRC), and superior frontal cortex (SFC). For the PCC, the FreeSurfer region called the isthmus cingulate cortex was used. These ROIs were chosen based on their involvement in early to late phases of Aβ and tau accumulation in AD [12, 13]. Specifically, the ERC and HPC represent early stages of tau deposition, whereas the PCC and PRC represent early stages of Aβ deposition. The MTC and SFC represent intermediate and late stages, respectively, of both Aβ and tau deposition. We also selected the ROIs so that a variety of different cytoarchitecture could be included in our analysis. We believed that the natural cellular composition of the region can play a role in determining the texture feature that changes in response to the Aβ and/or tau burden. The HPC belongs to the allocortex, which consists of three cellular laminae; the ERC belongs to the periallocortex, which is a transitional zone between the allocortex and neocortex; the MTC, PCC, PRC, and SFC belong to the neocortex, which consist of six laminae.

MRI processing

In ADNI 3, all T1-weighted images are corrected on-scanner for nonuniformity, no longer requiring offline preprocessing. We downloaded the T1-weighted images of each participant, resliced them to isovoxels ($1 \times 1 \times 1$ mm^3), and used FreeSurfer 6.0 (surfer.nmr.mgh.harvard.edu/) to parcellate them into brain regions as defined by the Desikan-Killiany atlas. For each participant, we mapped their brain parcellation mask from FreeSurfer space to the isovoxel native space, and extracted bilateral masks for each brain ROI. We used the bilateral masks to extract ROI images for each of the seven regions, with the original signal intensity values from each participant's T1-weighted image.

Each ROI image of each participant was further preprocessed prior to texture analysis as follows. We first normalized the histogram of each ROI image by removing any outlier voxels with intensity values beyond the $(\mu - 3\sigma, \mu + 3\sigma)$ range (where μ and σ signify mean signal intensity of the ROI and its standard deviation, respectively) to guard against partial volume effects [16]. Next, we normalized each gray matter voxel with respect to the participant's mean cerebrospinal fluid signal intensity in the lateral ventricle regions. This was done to correct

for any interindividual variations in scaling factors, because considerable variation in the scales can still exist even from a single MRI scan platform [17]. Finally, we performed quantization in each ROI image, rescaling all signal intensity values to a uniform range of 1–32. This step is commonly performed prior to texture analysis to reduce the number of gray levels to a smaller range of discrete values and thereby avoid statistical problems related to sparse matrices during the calculation of texture features. Throughout the preprocessing process we did not perform any spatial normalization, to avoid introducing any artifacts or distorting original intensity variations.

In each preprocessed ROI image, we conducted three-dimensional (3D) gray-level co-occurrence matrix (GLCM) analysis [18, 19] to extract texture features [18, 20] that characterize spatial patterns of gray-level distribution in the image.

GLCM texture analysis

Briefly, the GLCM is a $N \times N$ matrix where N is the total number of gray levels in the image (i.e., 32) and where each element, $p(i,j)$, of this matrix records the frequency of a certain voxel pairing (consisting of a reference voxel of value i and a neighboring voxel of value j) occurring within the ROI. The neighboring voxel can be defined based on various offsets of distance d and direction (ϕ,θ) with respect to the reference voxel. A GLCM is defined for each type of specified offset. In this study, we looked at voxel pairs of within $d = 1$ of each other (directly adjacent voxels) in 13 different directions, resulting in 13 GLCMs per ROI. The 13 GLCMs look at voxel pairs not only on the same slice but also from adjacent slices, allowing us to look at spatial relations of voxels in 3D space. Each GLCM is normalized so that the frequency of each voxel pair is divided by the total number of voxels in the ROI. In essence, the probability of value i and value j co-occurring in a defined offset distance d and direction (ϕ,θ) in the ROI is recorded in each of the 13 GLCMs. They are then collapsed into one average GLCM, which contains compact information about the image's spatial intensity patterns.

Haralick texture features, which are mathematical equations that utilize the average GLCM as input, are then calculated. Four features that uniquely characterize a different aspect of the image's signal intensity composition were calculated in this study. In total, 24 texture features (four texture features × six ROIs) were calculated in each participant. The four texture features—entropy, contrast, autocorrelation, and cluster shade—are simple, interpretable, and intuitive. Entropy reflects the randomness of spatial distribution of gray levels without regard to the intensity of those voxels, whereas contrast reflects both the spatial distribution and the relative difference in intensities of neighboring voxels. Specifically, contrast becomes higher when neighboring voxels have very different intensities (expected in a sharp, heterogeneous image) compared to having very similar intensities (expected in a solid tone, homogenous image). Autocorrelation reflects the overall brightness/darkness as well as fineness/coarseness of an image. Cluster shade reflects asymmetry of the proportion of relatively bright and dark intensities in the image, with the sign indicating the direction of the asymmetry (i.e., a negative value corresponds to a higher proportion of brighter voxels than darker voxels in the image, and vice versa) and the absolute value representing the magnitude of asymmetry. The characteristics of these features are described in Table 1.

PET processing

To measure cerebral Aβ and tau burden, we downloaded fully preprocessed (Coreg, Avg, Std Img and Vox Siz, Uniform Resolution) AV45 PET images and AV1451 PET images, respectively, from the ADNI 3 database. We used PETSurfer [21] to perform MRI-PET coregistration and calculate partial volume effects-corrected standardized uptake value ratios (SUVR) in each ROI, using uptake in the whole cerebellum as a reference region.

Statistical analysis

We examined the associations of texture features with Aβ burden and tau burden in each region using linear regression analyses, in which regional texture features were computed as the dependent variable, regional AV45 uptake and AV1451 uptake as the independent variables, and age and sex as covariates. Although ROI volume could be a possible factor contributing to the texture features, we did not include it as a covariate because GLCM texture measures are normalized to the total number of voxels in the ROI, which would adjust for such volumetric differences. We repeated the same analysis with regional mean signal intensity (derived after normalization to the participant's mean ventricle signal intensity) as the dependent variable. We also compared the regional Aβ and tau burdens, texture features, and mean signal intensities between in vivo Braak stages using analysis of variance (ANOVA) with Bonferroni post hoc comparisons. We performed all analyses using the Statistical Package for the Social Sciences (SPSS) for Windows (version 22.0; IBM), and considered a two-sided p value <0.05 as statistically significant.

RESULTS

Study participant demographics

The characteristics of the 150 participants (78 men aged 76.5 ± 7.2 years and 72 women aged 74.6 ± 8.0 years) are summarized in Table 2. They consisted of 121 Aβ-negative participants (84 CN, 37 MCI) and 29 Aβ-positive participants (11 CN, 14 MCI, four AD). In the in vivo Braak staging, 12 participants (2/4 AD, 8/51 MCI, 1/95 CN) were in stage V/VI (Braak V/VI mean SUVR > 1.582), VII (2/4 AD, 3/51 MCI, 3/95 CN) in stage III/VI (Braak III/IV mean SUVR > 0.504), 19 (9/51 MCI, 10/95 CN) in stage I/II (Braak I/II mean SUVR > 1.489), and the remaining 112 (31/51 MCI, 81/95 CN) in stage 0. As the number of participants assigned to III/IV was too small, we pooled the participants assigned to stages III/IV and V/VI into stage III/IV/V/VI ($n = 19$). Between the Braak stage groups, the proportion of females

TABLE 1 Haralick texture features

Feature	Formula[a]	Description
Entropy	$-\sum_i \sum_j p(i,j)\log(p(i,j))$	Measures randomness/uncertainty of gray-level distribution (spatial disorder) without regard to the intensity of those voxels. Solid tone image would have an entropy value of 0.
Contrast	$\sum_i \sum_j \lvert i-j\rvert^2 \cdot p(i,j)$	Measures local gray level variation in an image. Reflects both the spatial distribution and the relative difference in intensities of neighboring voxels. Heavy textures (greater disparity in intensity values between neighboring voxels, expected in a sharp, heterogeneous image) give high values and smooth, soft textures (expected in a solid tone, homogenous image) give low values.
Autocorrelation	$\sum_i \sum_j (ij)p(i,j)$	Measures the magnitude of the fineness and coarseness of texture. Textures with more pairs of high gray levels give higher values.
Cluster shade	$\sum_i \sum_j (i+j-\mu_x-\mu_y)^3 p(i,j)$	Measures skewness of the GLCM. Reflects asymmetry of the proportion of relatively bright and dark intensities in the image, with the sign indicating the direction of the asymmetry (i.e., a negative value corresponds to a higher proportion of brighter voxels than darker voxels in the image, and vice versa) and the absolute value representing the magnitude of asymmetry.

Note: [a]$p(i,j)$, (i,j)th entry in a normalized gray-level co-occurrence matrix; N_g, number of distinct gray levels in the quantized image; $\sum_i$, $\sum_{i=1}^{Ng}$, $\sum_j$, $\sum_{j=1}^{Ng}$; μx, mean of px; μy, mean of p_y; σ_x, standard deviation of p_x; σy, standard deviation of p_y.

Abbreviation: GLCM, gray-level co-occurrence matrix.

TABLE 2 Characteristics of the participants

Characteristics	All, n = 150	Aβ-negative, n = 121	Aβ-positive, n = 29
Age, years, mean (SD)	75.6 (7.7)	75.3 (7.5)	77.0 (8.4)
Female, %	48.0%	50.4%	37.9%
In vivo Braak stage, %			
Stage 0	74.7%	86.0%	27.6%
Stage I–II	12.7%	10.7%	20.7%
Stage III–VI	12.6%	3.3%	51.7%
Clinical state, %			
Cognitively normal	63.3%	69.4%	37.9%
Mild cognitive impairment	34.0%	30.6%	48.3%
Dementia	2.7%	0.0%	13.8%
Days between MRI and AV45, mean (SD)	18.7 (20.2)	19.8 (21.5)	14.3 (13.1)
Days between MRI and AV1451, mean (SD)	22.5 (22.5)	24.5 (22.9)	14.1 (18.7)
Days between AV45 and AV1451, mean (SD)	12.5 (16.7)	13.0 (17.6)	10.5 (12.6)

Abbreviations: Aβ, amyloid β; AD, Alzheimer's disease; AV45, florbetapir positron emission tomography; AV1451, flortaucipir positron emission tomography; MRI, magnetic resonance imaging; SD, standard deviation.

was comparable (48.2% in Braak stage 0, 52.6% in Braak stage I/II, 42.1% in Braak stage III/IV/V/VI, F = 0.21, p = 0.81, ANOVA), but the mean age was different (74.5 ± 7.2 years old in Braak stage 0, 83.2 ± 4.9 years old in Braak stage I/II, 74.7 ± 8.4 years old in Braak stage III/IV/V/VI, F = 12.27, p < 0.001, ANOVA).

Associations between MRI texture, signal intensity, and AD pathology

As summarized in Table 3, regional texture features were associated with regional tau burden but not with regional Aβ burden in all regions. The kind of texture features that were associated with tau burden were different between regions, which notably corresponded to the cytoarchitecture of the region. In the HPC, which is an allocortical region, autocorrelation was positively associated with tau burden (B = 18.11, p < 0.001), and cluster shade was negatively associated with tau burden (B = −266.28, p < 0.001). However, neither entropy nor contrast was associated with tau burden. Meanwhile, in neocortical regions such as the MTC, PCC, PRC, and SFC, entropy (B = 0.27, p = 0.009; B = 0.04, p = 0.008; B = 0.03, p = 0.05; B = 0.05, p = 0.04, respectively) and contrast (B = 3.12, p = 0.003; B = 2.41, p = 0.007; B = 1.79, p = 0.04; B = 3.01, p = 0.03, respectively) were positively associated with tau burden, whereas autocorrelation and cluster shade were not.

TABLE 3 Associations of the regional texture features with the regional amyloid β and tau burdens

	Entropy		Contrast		Autocorrelation		Cluster shade		Mean signal intensity	
	B **(SE)**	***β***	***B*** **(SE)**	***β***	***B*** **(SE)**	***β***	***B*** **(SE)**	***β***	***B*** **(SE)**	***β***
Hippocampus										
Aβ	0.03 (0.10)	0.03	−2.59 (4.89)	−0.05	−14.71 (12.08)	−0.09	9.11 (158.31)	0.00	−0.07 (0.29)	−0.02
Tau	−0.05 (0.03)	−0.13	−1.59 (1.53)	−0.09	18.11 (3.77)***	0.38	−266.28 (49.43)***	−0.41	0.07 (0.09)	0.07
Entorhinal Ctx										
Aβ	0.06 (0.03)	0.14	2.43 (2.42)	0.09	−3.16 (3.97)	−0.07	25.26 (32.43)	0.07	0.10 (0.10)	0.08
Tau	0.03 (0.01)**	0.26	2.35 (0.89)**	0.22	1.93 (1.46)	0.12	−42.39 (11.91)***	**−0.30**	−0.01 (0.04)	−0.02
Middle temporal Ctx										
Aβ	−0.02 (0.02)	−0.07	−0.33 (1.28)	−0.03	−0.74 (2.10)	−0.04	−2.80 (26.46)	−0.01	−0.02 (0.07)	−0.03
Tau	0.05 (0.02)**	0.27	3.12 (1.02)**	0.31	2.52 (1.67)	0.15	−16.92 (21.00)	−0.08	0.02 (0.06)	0.04
Posterior cingulate Ctx										
Aβ	−0.01 (0.02)	−0.04	0.75 (1.24)	0.06	1.80 (3.36)	0.05	−9.47 (43.38)	−0.02	0.08 (0.07)	0.11
Tau	0.04 (0.02)**	0.26	2.41 (0.88)**	0.26	−1.47 (2.39)	−0.06	9.80 (30.89)	0.03	0.00 (0.05)	0.01
Precuneus										
Aβ	0.01 (0.02)	0.05	0.28 (1.02)	0.03	2.30 (2.93)	0.08	−32.16 (23.74)	−0.14	0.04 (0.05)	0.08
Tau	0.03 (0.02)	0.18	1.79 (0.88)*	0.20	0.84 (2.51)	0.03	15.46 (20.31)	0.08	−0.02 (0.04)	−0.04
Superior frontal Ctx										
Aβ	−0.00 (0.02)	−0.02	−1.17 (0.94)	−0.11	−0.46 (1.22)	−0.03	44345 (24.89)	0.17	−0.01 (0.04)	−0.03
Tau	0.05 (0.03)*	0.20	3.01 (1.37)*	0.20	1.83 (1.78)	0.09	−45.94 (36.27)	−0.12	0.07 (0.06)	0.10

Note: Linear regression analysis adjusting for age and sex.

Abbreviations: Aβ, amyloid-β; *B*, unstandardized beta coefficients; *β*, standardized beta coefficient; Ctx, cortex; SE, standard error.

***$p < 0.001$; **$p < 0.01$; *$p < 0.05$.

In the ERC which is a periallocortical region, entropy and contrast were positively ($B = 0.03$, $p = 0.002$; $B = 2.35$, $p = 0.009$, respectively) and cluster shade was negatively ($B = -42.39$, $p < 0.001$) associated with tau burden. Mean signal intensity did not show associations with neither Aβ nor tau in all regions. The linear regression analyses were conducted again using bootstrapped analysis to ensure the results were not chance findings (Table S1). Tau burdens were different between the regions of different cytoarchitectures ($p < 0.001$ by repeated measures ANOVA). In the post hoc comparisons, tau burdens were different between all regions except between HPC and PRC ($p = 0.29$) and between PCC and SFC ($p = 0.93$).

Braak stage group differences in neuroimaging measures

In all regions, higher Braak stage groups tended to have higher Aβ and tau burdens; higher entropy, contrast and autocorrelation; and lower cluster shade values compared to lower stage groups (Table 4). In the HPC and ERC, cluster shade was lower, and entropy and autocorrelation were higher in stage I/II and/or stage III–VI groups compared to the stage 0 group. In the ERC, entropy and contrast were higher in stage III–VI groups compared to the stage 0 group. In the PRC, contrast and entropy were higher in stage I/II and stage III-VI groups, respectively, compared to the stage 0 group. In the MTC, PCC, and SFC, all texture features were comparable between Braak stages. Mean signal intensity in all regions were not statistically different between Braak stage groups.

DISCUSSION

This study was conducted to elucidate the relationship between texture of brain MRI and AD pathology, which has not been investigated before. This study demonstrated for the first time in humans that regional texture features of T1-weighted brain MRI may reflect brain tissue changes related to regional tau burden but not Aβ burden, and that this texture value can change further as AD progresses.

Although no study has yet investigated pathological correlates of MRI texture in humans, one mouse study found that there are differences in MRI texture between wild-type mice and rTg4510 transgenic mice, and that MRI texture correlates well with histological measurements of tau burden in the cortex, hippocampus, and thalamus [22]. In the current study, we found that MRI texture is associated with tau burden in humans as well. The absence of a

TABLE 4 Comparisons of regional amyloid β burden, tau burden, texture features, and mean signal intensity between in vivo Braak stages

Region and imaging measures	Stage 0[a], *n* = 112	Stage I–II[b], *n* = 19	Stage III–VI[c], *n* = 19	Statistics[*]		
				F	*p* value	Post hoc
Hippocampus						
Aβ burden	0.63 (0.07)	0.68 (0.09)	0.71 (0.07)	10.77	<0.001	a < c
Tau burden	1.19 (0.13)	1.56 (0.21)	1.73 (0.32)	100.49	<0.001	a < b < c
Entropy	5.79 (0.10)	5.73 (0.09)	5.78 (0.09)	2.97	0.06	a < b
Contrast	30.28 (4.81)	29.85 (3.83)	29.80 (4.01)	0.13	0.88	–
Autocorrelation	272.02 (9.69)	278.49 (12.47)	280.21 (23.90)	4.85	0.009	a < c
Cluster shade	−74.82 (151.20)	−222.32 (169.34)	−247.12 (210.46)	13.96	<0.001	a > b, c
Mean signal intensity	2.70 (0.31)	2.70 (0.29)	2.72 (0.22)	0.04	0.97	–
Entorhinal cortex						
Aβ burden	0.56 (0.19)	0.65 (0.28)	0.77 (0.32)	7.49	0.001	a < c
Tau burden	1.35 (0.25)	1.87 (0.33)	2.70 (1.06)	78.79	<0.001	a < b < c
Entropy	5.90 (0.10)	5.93 (0.06)	5.96 (0.08)	5.20	0.007	a < c
Contrast	29.87 (6.88)	33.97 (4.05)	34.12 (5.61)	5.95	0.003	a < b, c
Autocorrelation	267.79 (9.60)	273.89 (12.52)	273.05 (12.25)	4.30	0.02	–
Cluster shade	26.47 (82.48)	−74.75 (87.97)	−67.77 (63.20)	20.65	<0.001	a> b, c
Mean signal intensity	2.43 (0.29)	2.49 (0.28)	2.45 (0.24)	0.36	0.70	–
Middle temporal cortex						
Aβ burden	0.64 (0.24)	0.84 (0.29)	1.22 (0.41)	36.42	<0.001	a < b < c
Tau burden	1.36 (0.18)	1.46 (0.13)	2.34 (0.60)	111.76	<0.001	a, b < c
Entropy	5.82 (0.08)	5.84 (0.06)	5.85 (0.06)	1.74	0.18	–
Contrast	23.94 (4.30)	26.26 (3.47)	26.26 (3.98)	4.40	0.01	–
Autocorrelation	272.80 (6.57)	273.32 (4.63)	276.25 (9.26)	2.28	0.11	–
Cluster shade	−59.27 (90.66)	−86.11 (82.76)	−88.77 (79.46)	1.45	0.24	–
Mean signal intensity	2.24 (0.24)	2.29 (0.21)	2.26 (0.19)	0.34	0.71	–
Posterior cingulate cortex						
Aβ burden	0.62 (0.25)	0.79 (0.36)	1.13 (0.41)	29.19	<0.001	a, b < c
Tau burden	1.08 (0.17)	1.25 (0.14)	2.03 (0.88)	62.52	<0.001	a, b < c
Entropy	5.88 (0.07)	5.87 (0.06)	5.91 (0.05)	2.09	0.13	–
Contrast	27.66 (4.46)	29.62 (3.58)	29.78 (3.48)	3.27	0.04	–
Autocorrelation	266.72 (11.24)	265.78 (5.69)	270.60 (14.34)	1.13	0.33	–
Cluster shade	−15.39 (162.67)	−36.57 (68.32)	−46.99 (73.85)	0.49	0.61	–
Mean signal intensity	2.63 (0.25)	2.66 (0.26)	2.69 (0.15)	0.41	0.67	–
Precuneus						
Aβ burden	0.67 (0.31)	0.87 (0.39)	1.49 (0.50)	44.45	<0.001	a, b < c
Tau burden	1.21 (0.15)	1.35(0.13)	2.16 (1.13)	42.14	<0.001	a, b < c
Entropy	5.85 (0.08)	5.87 (0.08)	5.90 (0.09)	3.80	0.03	a < c
Contrast	23.04 (4.58)	25.95 (4.93)	25.54 (4.70)	4.86	0.009	a < b
Autocorrelation	281.46 (12.87)	281.30 (9.21)	287.89 (15.02)	2.11	0.12	–
Cluster shade	−98.64 (105.73)	−121.44 (110.74)	−114.51 (98.37)	0.50	0.61	–
Mean signal intensity	2.34 (0.23)	2.38 (0.24)	2.38 (0.17)	0.47	0.63	–
Superior frontal cortex						
Aβ burden	0.62 (0.29)	0.79 (0.43)	1.28 (0.39)	34.11	<0.001	a, b < c
Tau burden	1.17 (0.22)	1.28 (0.12)	1.54 (0.39)	20.69	<0.001	a, b < c

(Continues)

TABLE 4 (Continued)

Region and imaging measures	Stage 0[a], *n* = 112	Stage I–II[b], *n* = 19	Stage III–VI[c], *n* = 19	Statistics*		
				F	*p* value	Post hoc
Entropy	5.83 (0.07)	5.83 (0.07)	5.85 (0.06)	0.63	0.54	–
Contrast	24.37 (4.05)	25.99 (3.84)	24.81 (4.05)	1.34	0.27	–
Autocorrelation	269.25 (5.14)	270.12 (2.62)	271.97 (6.54)	2.38	0.10	–
Cluster shade	36.67 (108.50)	−20.60 (86.85)	26.62 (78.41)	2.52	0.08	–
Mean signal intensity	1.84 (0.17)	1.90 (0.19)	1.86 (0.11)	0.90	0.41	–

a, b, and c is to refer to those respective groups when showing the post hoc analysis.

*One-way analysis of variance with Bonferroni post hoc comparisons.

relationship between Aβ and texture in our study may reflect the fact that T2-weighted images, which are known to be sensitive to iron deposits associated with Aβ, were not used. Based on the observation that texture was only associated with tau and not with Aβ, which is larger in size, texture may not reflect the tau protein accumulation itself, but rather another microstructural change that is closely associated with the tau burden.

The direction of texture and signal intensity changes across the Braak stage groups suggest an increasing trend toward brighter voxels with increasing pathological burden (higher autocorrelation, lower cluster shade, higher signal intensity). This is a finding consistent with converging evidence that AD involves a remyelination process in the gray matter as a homeostatic response to myelin breakdown [23]. There have been in vivo and ex vivo findings of increased intracortical myelin content [24–26] and disorganized myeloarchitecture [24, 27] in AD patients compared to normal controls. The studies have further noted a visibly inhomogeneous band of hypointense T2*-weighted MRI signals across the cortex, which blurred the cortical laminae and was highly associated with myelin content. This band of disorganized myeloarchitecture is expected to be more pronounced in T1-weighted images, as T1 signals are strongly dependent on lipid concentration associated with myelin [28], and are expected to be reasonably detectable through quantitative methods such as texture analysis because it could be visibly observed on high-resolution MRI scans. Based on these previous reports, the texture differences observed in our study are likely to have a basis in such myeloarchitectural changes, and the tau-texture associations are likely to reflect the linear relationship between high tau and intracortical myelin content [25]. Although the brightening of voxels may be counterintuitive to the expectation that gray matter voxels would become darker in AD as a result of atrophy, it is possible that the AD-associated reduction in gray matter density reported in previous literature [29–32] reflects a growing amount of white matter–like tissue or myelinated gray matter in place of the normal gray matter tissue. Further studies on the changes in gray matter and white matter tissue will be needed to investigate this.

With respect to the tau-texture associations, the tau-associated texture feature showed a remarkable correspondence with the cytoarchitecture of the region. The six regions in our study are characterized by different types of cytoarchitecture, which differ in the number of laminae and the location of cells vulnerable to neurofibrillary tangles (NFTs) deposition. The regions in which entropy and contrast were affected by tau belong to the neocortex (i.e., MTC, PCC, PRC, SFC), which consists of six laminae; the HPC, in which autocorrelation and cluster shade were affected, belongs to the allocortex, which consists of three laminae; and the ERC, in which features common to both allocortex and neocortex were affected, belongs to a transitional area between the two. Furthermore, NFTs are known to preferentially affect different cells in different regions: the pyramidal neurons of layers III and V in the neocortex; the stellate neurons of layer II, superficial portion of layer III, and multipolar neurons of layer IV in the ERC; and the stratum pyramidale of cornu ammonis 1 and subiculum in the HPC [33–35]. Consequently, the different layout of the typically affected cell types can differentially affect the distribution of the voxel's signal intensity and therefore the kind of textural change (Figure 1). An extensive analysis including more regions further supported cytoarchitecture as the contributing factor of the differences in significant texture features among different regions (Tables S2 and S3). However, because the allocortical and periallocortical regions (HPC and ENT) in our study also correspond to the earliest stages of tau accumulation, there is a steep difference in AV1451 uptake between them and other neocortical regions. Thus, we cannot leave out the possibility that factors other than cytoarchitecture, such as the degree of local tau burden and/or other neurodegenerative changes, are driving the tau-texture patterns, and further studies will be needed to investigate this.

It is notable that although texture features were significantly associated with tau burden, mean signal intensity was not (Table 3). This suggests that early microstructural changes may be reflected as subtle changes in signal intensity that are not intense enough to be detected as first-order statistics such as mean intensity, but sufficient to be detected as second-order statistics such as texture. Although no individual texture feature alone is expected to be sufficient discriminators of AD from non-AD, optimal combinations of relevant texture features will be helpful [6, 7]. It is also worth noting that many studies on MRI-pathology associations have been conducted mainly on T2-weighted images, and few data on T1-weighted images are available. It will be of more clinical value to investigate these relationships in

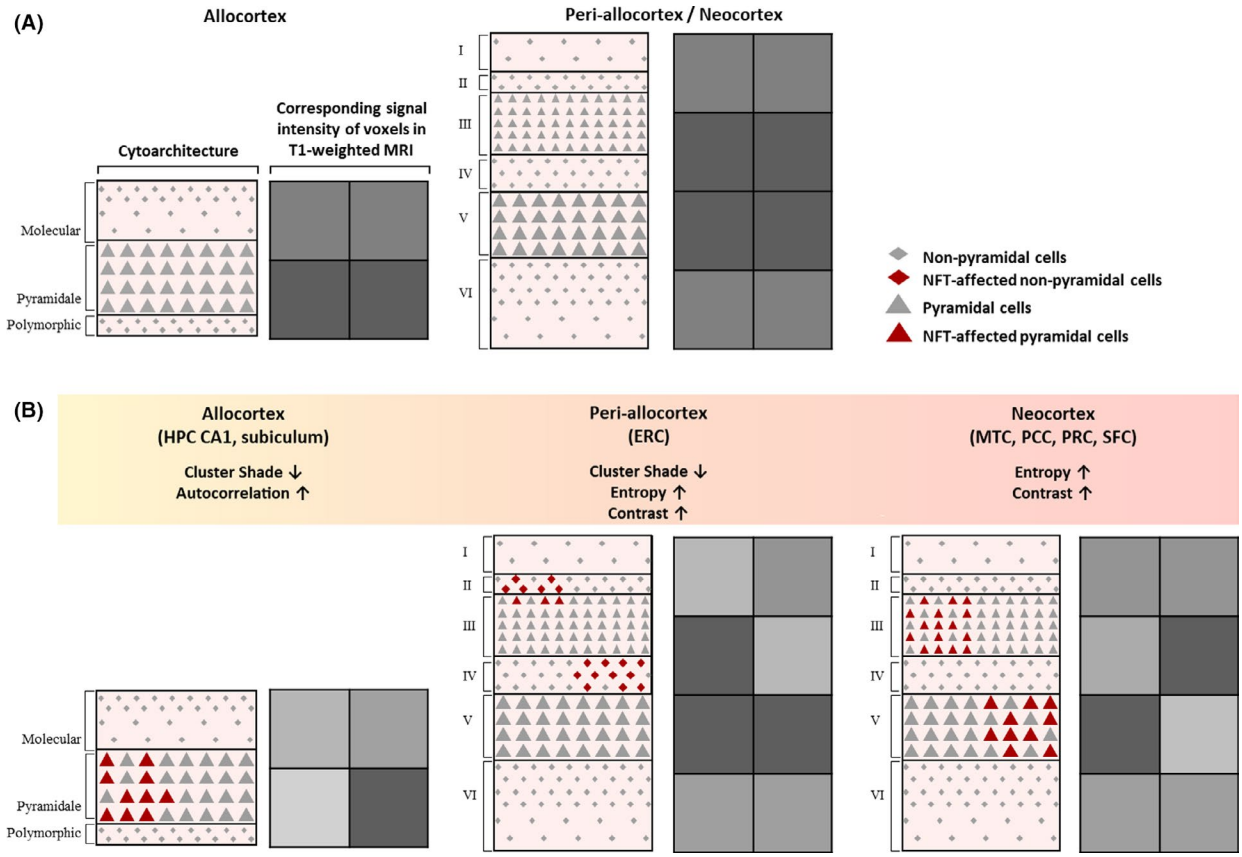

FIGURE 1 Schema of how different cytoarchitecture can affect tau-associated texture changes. Schematic drawings of the cytoarchitecture and corresponding signal intensities on T1-weighted images in healthy brain tissue (A) and NFT-accumulated brain tissue (B). Tau proteins are deposited as NFT in different cellular laminae according to the cytoarchitecture (allocortex, periallocortex, neocortex) of the brain region. Left: In the HPC, which is a unique structure that consists of rolled-up laminae of its subregions that are about two-voxels thick, tau-related microstructural changes along the pyramidal layers that are located laterally may result in an overall lightening and smoothening of the HPC signal intensities, thus increasing autocorrelation and decreasing both cluster shade and entropy. Center: In the ERC, which contains more neocortex-like laminar structure, there are textural changes that are similar to that in neocortices, with the slight difference in locations of the signal intensity changes possibly due to the slight difference in the locations of the NFT-affected layers. Right: In neocortical regions, which are typically four-voxels (voxel size: $1 \times 1 \times 1$ mm^3) thick, NFT-associated microstructural changes (i.e., myelin repair) may selectively change signal intensities of voxels of the inner two rows that correspond to NFT-affected cells in the pyramidal layers (dark triangles). These changes may increase the differences in the magnetic resonance signal intensities between neighboring inner and outer voxels throughout the neocortical laminae, thus increasing entropy and contrast of the region. Note that signal intensity changes in the figure are exaggerated for illustrative purposes. CA1, cornu ammonis 1; ERC, entorhinal cortex; HPC, hippocampus; MRI, magnetic resonance imaging; MTC, middle temporal cortex; NFT, neurofibrillary tangles; PCC, posterior cingulate cortex; PRC, precuneus; SFC, superior frontal cortex.

T1-weighted images, as they are more widely available in clinical settings.

This study has several limitations. First, there is a lack of sufficient late-stage AD participants in our sample, mainly due to the lack of follow-up data accumulated yet in ADNI 3. Second, our study was conducted on MRI scans from only one scanner platform, limiting the generalization of the results. Third, we did not directly measure the myelin contents. Future studies must address the effects of interscanner variability in texture analysis, as well as further validate what it reflects through histological samples when available.

In conclusion, texture of T1-weighted brain MRI may reflect microstructural changes related to tau accumulation in AD. This study supports further analysis of textures as MRI-based biomarkers of early microstructural changes.

ACKNOWLEDGMENTS

This research was supported by the grants from the Korean Health Technology R&D Project, Ministry of Health and Welfare, Republic of Korea (grant no. HI09C1379 [A092077]), and the Institute for Information & Communications Technology Promotion (IITP) grant funded by the Korea government (MSIT) (2018-2-00861, Intelligent SW Technology Development for Medical Data Analysis). Data collection and sharing for this project was funded by the Alzheimer's Disease Neuroimaging Initiative (ADNI) (National Institutes of Health Grant U01 AG024904) and DOD ADNI (Department of Defense award number

W81XWH-12-2-0012). ADNI is funded by the National Institute on Aging, the National Institute of Biomedical Imaging and Bioengineering, and through generous contributions from the following: AbbVie, Alzheimer's Association; Alzheimer's Drug Discovery Foundation; Araclon Biotech; BioClinica, Inc.; Biogen; Bristol-Myers Squibb Company; CereSpir, Inc.; Cogstate; Eisai Inc.; Elan Pharmaceuticals, Inc.; Eli Lilly and Company; EuroImmun; F. Hoffmann-La Roche Ltd and its affiliated company Genentech, Inc.; Fujirebio; GE Healthcare; IXICO Ltd.; Janssen Alzheimer's Immunotherapy Research & Development, LLC.; Johnson & Johnson Pharmaceutical Research & Development LLC.; Lumosity; Lundbeck; Merck & Co., Inc.; Meso Scale Diagnostics, LLC.; NeuroRx Research; Neurotrack Technologies; Novartis Pharmaceuticals Corporation; Pfizer Inc.; Piramal Imaging; Servier; Takeda Pharmaceutical Company; and Transition Therapeutics. The Canadian Institutes of Health Research is providing funds to support ADNI clinical sites in Canada. Private sector contributions are facilitated by the Foundation for the National Institutes of Health (www.fnih.org). The grantee organization is the Northern California Institute for Research and Education, and the study is coordinated by the Alzheimer's Therapeutic Research Institute at the University of Southern California. ADNI data are disseminated by the Laboratory for Neuro Imaging at the University of Southern California.

CONFLICTS OF INTEREST

The authors declare that there are no conflicts of interest associated with this work.

DATA AVAILABILITY STATEMENT

The data that support the findings of this study are available from the corresponding author upon reasonable request.

ORCID

Ki Woong Kim https://orcid.org/0000-0002-1103-3858

REFERENCES

1. de Oliveira MS, Balthazar ML, D'Abreu A, et al. MR imaging texture analysis of the corpus callosum and thalamus in amnestic mild cognitive impairment and mild Alzheimer disease. *Am J Neuroradiol*. 2011;32:60–66.
2. Xia H, Tong L, Zhou X, Zhang J, Zhou Z, Liu W.Texture Analysis and Volumetry of Hippocampus and Medial Temporal Lobe in Patients with Alzheimer's Disease. Paper presented at: 2012 International Conference on Biomedical Engineering and Biotechnology; 28–30 May 2012, 2012.
3. Chincarini A, Bosco P, Calvini P, et al. Local MRI analysis approach in the diagnosis of early and prodromal Alzheimer's disease. *NeuroImage*. 2011;58:469–480.
4. Feng F, Wang P, Zhao K, et al. Radiomic features of hippocampal subregions in Alzheimer's disease and amnestic mild cognitive impairment. *Front Aging Neurosci*. 2018;10:290.
5. Freeborough PA, Fox NC. MR image texture analysis applied to the diagnosis and tracking of Alzheimer's disease. *IEEE Trans Med Imaging*. 1998;17:475–478.
6. Lee S, Lee H, Kim K. Magnetic resonance imaging texture predicts progression to dementia due to Alzheimer disease earlier than hippocampal volume. *J Psychiatry Neurosci*. 2019;44:1–8.
7. Luk CC, Ishaque A, Khan M, et al. Alzheimer's disease: 3-Dimensional MRI texture for prediction of conversion from mild cognitive impairment. *Alzheimers Dement (Amst)*. 2018;10:755–763.
8. Nanni L, Brahnam S, Salvatore C, Castiglioni I. Texture descriptors and voxels for the early diagnosis of Alzheimer's disease. *Artif Intell Med*. 2019;97:19–26.
9. Sørensen L, Igel C, Hansen NL, et al. Early detection of Alzheimer's disease using mri hippocampal texture. *Hum Brain Mapp*. 2016;37:1148–1161.
10. Deoni SCL. Quantitative relaxometry of the brain. *Top Magn Reson Imaging*. 2010;21:101–113.
11. Eickhoff S, Walters NB, Schleicher A, et al. High-resolution MRI reflects myeloarchitecture and cytoarchitecture of human cerebral cortex. *Hum Brain Mapp*. 2005;24:206–215.
12. Braak H, Alafuzoff I, Arzberger T, Kretzschmar H, Del Tredici K. Staging of Alzheimer disease-associated neurofibrillary pathology using paraffin sections and immunocytochemistry. *Acta Neuropathol*. 2006;112:389–404.
13. Mattsson N, Palmqvist S, Stomrud E, Vogel J, Hansson O. Staging β-amyloid pathology with amyloid positron emission tomography. *JAMA Neurol*. 2019;76(11):1319–1329.
14. Buch K, Kuno H, Qureshi MM, Li B, Sakai O. Quantitative variations in texture analysis features dependent on MRI scanning parameters: a phantom model. *J Appl Clin Med Phys*. 2018;19:253–264.
15. Schöll M, Lockhart SN, Schonhaut DR, et al. PET imaging of tau deposition in the aging human brain. *Neuron*. 2016;89:971–982.
16. Collewet G, Strzelecki M, Mariette F. Influence of MRI acquisition protocols and image intensity normalization methods on texture classification. *Magn Reson Imaging*. 2004;22:81–91.
17. Westlye LT, Walhovd KB, Dale AM, et al. Differentiating maturational and aging-related changes of the cerebral cortex by use of thickness and signal intensity. *NeuroImage*. 2010;52:172–185.
18. Haralick RM, Shanmugam K, Dinstein Ih. Textural features for image classification. *IEEE Trans Syst Man Cybern*. 1973;6:610–621.
19. Ortiz A, Palacio AA, Górriz JM, Ramírez J, Salas-González D. Segmentation of brain MRI using SOM-FCM-based method and 3D statistical descriptors. *Comput Math Methods Med*. 2013;2013:1–12.
20. Conners RW, Trivedi MM, Harlow CA. Segmentation of a high-resolution urban scene using texture operators. *Comput Vis Gr Image Process*. 1984;25:273–310.
21. Greve DN, Salat DH, Bowen SL, et al. Different partial volume correction methods lead to different conclusions: An 18F-FDG-PET study of aging. *NeuroImage*. 2016;132:334–343.
22. Colgan N, Ganeshan B, Harrison IF, et al. In vivo imaging of tau pathology using magnetic resonance imaging textural analysis. *Front Neurosci*. 2017;11:599.
23. Bartzokis G. Alzheimer's disease as homeostatic responses to age-related myelin breakdown. *Neurobiol Aging*. 2011;32:1341–1371.
24. Bulk M, Abdelmoula WM, Nabuurs RJA, et al. Postmortem MRI and histology demonstrate differential iron accumulation and cortical myelin organization in early- and late-onset Alzheimer's disease. *Neurobiol Aging*. 2018;62:231–242.
25. Pelkmans W, Dicks E, Barkhof F, et al. Gray matter T1-w/T2-w ratios are higher in Alzheimer's disease. *Hum Brain Mapp*. 2019;40:3900–3909.
26. Yasuno F, Kazui H, Morita N, et al. Use of T1-weighted/T2-weighted magnetic resonance ratio to elucidate changes due to amyloid β accumulation in cognitively normal subjects. *NeuroImage Clin*. 2017;13:209–214.
27. Kenkhuis B, Jonkman LE, Bulk M, et al. 7T MRI allows detection of disturbed cortical lamination of the medial temporal lobe in patients with Alzheimer's disease. *NeuroImage Clin*. 2019;21:101665.

28. Leuze C, Aswendt M, Ferenczi E, et al. The separate effects of lipids and proteins on brain MRI contrast revealed through tissue clearing. *NeuroImage*. 2017;156:412–422.
29. Casanova R, Whitlow CT, Wagner B, et al. High dimensional classification of structural MRI Alzheimer's disease data based on large scale regularization. *Front Neuroinform*. 2011;5:22.
30. Fan Y, Batmanghelich N, Clark CM, Davatzikos C. Initiative AsDN. Spatial patterns of brain atrophy in MCI patients, identified via high-dimensional pattern classification, predict subsequent cognitive decline. *NeuroImage*. 2008;39:1731–1743.
31. Klöppel S, Stonnington CM, Chu C, et al. Automatic classification of MR scans in Alzheimer's disease. *Brain*. 2008;131:681–689.
32. Vemuri P, Whitwell JL, Kantarci K, et al. Antemortem MRI based STructural Abnormality iNDex (STAND)-scores correlate with postmortem Braak neurofibrillary tangle stage. *NeuroImage*. 2008;42:559–567.
33. Arnold SE, Hyman BT, Flory J, Damasio AR, Van Hoesen GW. The topographical and neuroanatomical distribution of neurofibrillary tangles and neuritic plaques in the cerebral cortex of patients with Alzheimer's disease. *Cereb Cortex*. 1991;1:103–116.
34. Braak H, Braak E. Neuropathological stageing of Alzheimer-related changes. *Acta Neuropathol*. 1991;82:239–259.
35. Hyman BT, Van Hoesen GW, Damasio AR, Barnes CL. Alzheimer's disease: cell-specific pathology isolates the hippocampal formation. *Science*. 1984;225:1168.

SUPPORTING INFORMATION

Additional supporting information may be found online in the Supporting Information section.

How to cite this article: Lee S, Kim KW. Associations between texture of T1-weighted magnetic resonance imaging and radiographic pathologies in Alzheimer's disease. *Eur J Neurol*. 2020;00:1–10. https://doi.org/10.1111/ene.14609